Advanced Dual-Atom Catalysts on Graphitic Carbon Nitride for Enhanced Hydrogen Evolution via Water Splitting

Xinghui Liu,[a] Dang Kim Hoang,[b] Quynh Anh T. Nguyen,[b] Do Dinh Phuc,[c] Seong-Gon Kim,[d] Pham Cam Nam,[e] Ashwani Kumar,[f] Fuchun Zhang,[g] Chunyi Zhi,[h] and Viet Q. Bui*[b]

[a] School of Physics and Electronic Information, Yan'an University, Yan'an 716000, China; Science and Technology on Aerospace Chemical Power Laboratory, Hubei Institute of Aerospace Chemotechnology, Xiangyang 441003, China; Department of Materials Science and Engineering, City University of Hong Kong, 83 Tat Chee Avenue, Kowloon, Hong Kong SAR, China.

[b] Advanced Institute of Science and Technology, The University of Danang, 41 Le Duan, Danang, Vietnam.

[c] Department of Chemistry, Sungkyunkwan University, Suwon, 16419, Republic of Korea.

[d] Department of Physics & Astronomy and Center for Computational Sciences, Mississippi State University, Starkville, Mississippi 39762, United States.

[e] Faculty of Chemical Engineering, The University of Danang-University of Science and Technology, Danang City 550000, Vietnam.

[f] Max-Planck-Institut für Kohlenforschung, 45470 Mülheim an der Ruhr, Germany.

[g] School of Physics and Electronic Information, Yan'an University, Yan'an 716000, China.

[h] Department of Materials Science and Engineering, City University of Hong Kong, 83 Tat Chee Avenue, Kowloon, Hong Kong SAR, China.

* Corresponding author: Viet Q.Bui; E-mail: mrbuiquocviet@gmail.com; bqviet@ac.udn.vn

Table S1. Bader charge and magnetic moment analysis for dual-atom catalysts (DACs) in MN-gCN Structures. This table presents the Bader charge values for metal atoms M and N, their sum, and the average magnetic moment (Avg_μ_B) of MN-gCN configurations.

DACs (MN)	Bader charge of M (e)	Bader charge of N (e)	Sum (e)	Avg_μ_B (MN-gCN) (μ_B)
CrFe	1.293	0.120	1.413	3.314
FeFe	0.807	0.724	1.530	3.705
FeCu	0.834	0.554	1.388	3.102
FeNi	0.815	0.519	1.333	1.942
CoIr	0.932	-0.148	0.784	1.482
MnCo	0.546	0.654	1.200	3.564
CoRu	0.503	0.507	1.010	2.507
CoPt	0.563	0.421	0.984	0.559
CoCo	0.630	0.633	1.263	1.558
CoNi	0.625	0.471	1.095	0.374
FeCo	0.511	0.649	1.160	2.341
CrCo	1.013	0.498	1.510	2.488
CoCu	0.605	0.596	1.201	0.000
CoPd	0.647	0.462	1.110	0.000
CrPd	0.824	0.489	1.313	3.399
CuPd	0.529	0.618	1.148	0.082
MnPd	0.648	0.447	1.095	2.671
NiPd	0.581	0.588	1.170	0.000
FePd	0.969	0.361	1.330	2.009
PdPd	0.643	0.551	1.194	0.000
CrMn	0.989	0.695	1.683	0.103
MnCu	0.996	0.455	1.451	3.163
MnNi	1.100	0.165	1.264	2.672
MnMn	0.723	0.816	1.540	1.764
MnFe	0.843	0.497	1.340	2.375
PtPt	0.406	0.434	0.840	0.000
CuPt	0.590	0.098	0.688	0.000
NiPt	0.532	0.192	0.724	0.000
MnPt	0.566	0.591	1.157	2.829
FePt	0.973	-0.240	0.733	1.995
PdPt	0.296	0.203	0.500	0.000
CrPt	0.415	-0.792	-0.377	2.965
CrRu	0.823	0.608	1.431	1.496
FeRu	0.950	0.691	1.641	0.007
NiRu	0.644	0.631	1.275	1.312
CuRu	0.110	0.828	0.938	0.001
MnRu	0.880	0.142	1.022	2.335
PdRu	0.273	0.621	0.894	0.000
PtRu	0.230	0.777	1.007	0.000
RuRu	0.464	0.582	1.046	0.000
IrIr	0.733	0.760	1.493	0.000
NiIr	0.450	0.464	0.914	0.000

PtIr	0.470	0.225	0.696	0.000
MnIr	0.756	0.280	1.036	3.402
PdIr	0.473	0.048	0.521	0.000
FeIr	0.944	0.021	0.965	2.641
CuIr	0.762	-0.242	0.520	0.000
RuIr	0.806	0.356	1.162	0.123
CrNi	1.144	-0.026	1.118	3.700
NiNi	0.314	0.559	0.873	0.000
NiCu	0.339	0.148	0.487	-0.961
CrIr	0.922	0.421	1.344	2.318
CrCr	0.705	0.834	1.539	0.300
CrCu	1.216	0.492	1.709	3.025
CuCu	0.457	0.616	1.073	0.029

Table S2 presents a comprehensive evaluation of the energetic characteristics of heteronuclear and homonuclear metal dimers anchored on gCN. It details the computed binding energies (E_b), indicative of the interaction strength between bimetallic single-atoms and the g-CN substrate, the formation energies (E_{form}) which reflect the stability of the constructed DACs, and the dissolution potentials (U_{diss}) that provide insights into the electrochemical durability of the catalysts under study.

M-N	E_b (eV)	E_{form} (eV)	U_{diss} (V)
FeNi	-5.222	-0.389	-0.154
CrIr	-5.868	-0.192	0.256
PdPt	-4.943	-0.380	1.273
MnFe	-4.479	-0.523	-0.543
FeCu	-4.246	-0.139	0.020
CrMn	-4.526	-0.948	-0.561
NiPt	-5.769	-0.613	0.768
CrNi	-5.105	-0.649	-0.254
CuPt	-4.715	-0.285	0.903
FePt	-5.506	-0.428	0.584
CrRu	-5.529	-0.042	-0.201
FeCo	-5.299	-0.278	-0.219
CoCo	-5.423	-0.137	-0.208
CuPd	-3.841	-0.248	0.789
MnIr	-5.863	-0.610	0.400
NiIr	-6.235	-0.104	0.519
FeIr	-6.117	-0.064	0.401
CrCo	-5.032	-0.389	-0.394
MnRu	-5.512	-0.447	-0.134
CrPt	-5.182	-0.481	0.380
MnNi	-5.099	-1.065	-0.181
CrFe	-4.458	-0.079	-0.630
CoPt	-5.635	-0.292	0.598
MnCo	-5.048	-0.826	-0.310
CoCu	-4.583	-0.210	0.138
CrCu	-4.220	-0.489	-0.034
NiCu	-4.558	-0.372	0.229
CrCr	-4.629	-0.628	-0.586
PtPt	-5.867	-0.467	1.413
CuCu	-3.726	-0.266	0.475
NiNi	-5.528	-0.617	0.052
PdPd	-4.085	-0.359	1.166
FePd	-4.573	-0.332	0.440
FeFe	-5.025	-0.270	-0.305
MnMn	-4.198	-1.041	-0.649
CoNi	-5.448	-0.350	-0.092
MnCu	-4.065	-0.757	-0.036
MnPd	-4.388	-0.947	0.382
MnPt	-5.287	-1.008	0.509
CoPd	-4.781	-0.275	0.493

NiPd	-4.866	-0.547	0.639
CrPd	-4.384	-0.521	0.304
PtRu	-6.017	0.170	0.732
CuIr	-5.397	0.008	0.744
CuRu	-4.909	0.307	0.245
PtIr	-6.272	0.103	1.099
FeRu	-5.715	0.149	-0.067
CoRu	-5.925	0.204	-0.013
IrIr	-3.495	3.856	-2.700
RuIr	-6.764	0.398	0.540
PdRu	-5.107	0.243	0.600
CoIr	-6.226	0.092	0.378
RuRu	-6.679	0.295	0.308
NiRu	-5.723	0.219	-0.011
PdIr	-5.433	0.105	1.002

Table S3. Transition metal interaction with hydrogen adsorbates. This table provides comprehensive data on the adsorption of hydrogen (H*) in combination with different transition metals (TMs) on MN-gCN surfaces. Each row lists a metal pair (MN), the distance between hydrogen and the transition metal (H-TM distance in Å), the Bader charge of the adsorbed hydrogen (H* Bader charge), the integrated crystal orbital Hamilton population (iCOHP) between H* and TM, magnetic moment (μ_B) for activated metal site, and the Gibbs free energy change (ΔG_{H*}) for hydrogen adsorption (in eV).

MN	H-TM distance (Å)	H* Bader charge (e)	H-TM iCOHP (eV)	μ_B (active site)	ΔG_{H*} (eV)
CrFe	1.566	-0.351	-0.903	2.083	-0.824
FeFe	1.610	-0.164	-0.839	2.218	-0.556
FeCu	1.609	-0.215	-0.840	2.931	-0.552
FeNi	1.621	-0.150	-0.822	2.469	-0.469
CoIr	1.511	-0.647	-0.936	1.395	-1.006
MnCo	1.532	-0.626	-0.944	0.419	-0.923
CoRu	1.539	-0.554	-0.915	1.482	-0.901
CoPt	1.544	-0.593	-0.910	0.958	-0.887
CoCo	1.559	-0.427	-0.888	1.080	-0.872
CoNi	1.577	-0.533	-0.910	0.792	-0.777
FeCo	1.568	-0.477	-0.900	0.805	-0.657
CrCo	1.559	-0.528	-0.896	-0.912	-0.656
CoCu	1.581	-0.495	-0.888	0.000	-0.619
CoPd	1.599	-0.482	-0.853	0.000	-0.514
CrPd	1.641	-0.347	-0.920	-0.060	-0.393
CuPd	1.652	-0.159	-0.908	0.022	-0.242
MnPd	1.677	-0.165	-0.803	-0.011	-0.165
NiPd	1.685	0.059	-0.827	0.000	-0.146
FePd	1.676	-0.205	-0.816	0.000	0.002
PdPd	1.682	0.080	-0.718	0.000	0.103
CrMn	1.658	-0.383	-0.914	-0.329	-0.660
MnCu	1.686	-0.367	-0.808	3.543	-0.526
MnNi	1.704	-0.234	-0.730	3.414	-0.407
MnMn	1.722	-0.137	-0.700	0.671	-0.316
MnFe	1.667	-0.228	-0.749	0.585	-0.267
PtPt	1.676	0.220	-1.044	0.000	-0.538
CuPt	1.647	-0.312	-1.059	0.000	-0.486
NiPt	1.667	-0.071	-1.039	0.000	-0.352
MnPt	1.631	-0.183	-1.069	0.014	-0.350
FePt	1.616	-0.209	-1.055	0.034	-0.268
PdPt	1.658	-0.093	-1.024	0.000	-0.248
CrPt	1.667	0.173	-1.012	-0.124	0.298
CrRu	1.601	-0.539	-1.331	-0.157	-0.955
FeRu	1.749	-0.290	-1.099	0.104	-0.840
NiRu	1.662	-0.512	-1.194	0.640	-0.777
CuRu	1.719	-0.514	-1.188	0.001	-0.626
MnRu	1.636	-0.384	-1.133	0.090	-0.514
PdRu	1.693	-0.225	-1.131	0.000	-0.387

PtRu	1.742	-0.158	-1.024	0.000	-0.343
RuRu	1.710	-0.154	-0.995	0.000	-0.218
IrIr	1.652	-0.423	-1.353	0.000	-1.071
NiIr	1.684	-0.584	-1.262	0.000	-0.943
PtIr	1.690	-0.544	-1.276	0.000	-0.936
MnIr	1.716	-0.614	-1.272	-0.002	-0.834
PdIr	1.727	-0.497	-1.143	0.000	-0.792
FeIr	1.731	-0.516	-1.214	0.272	-0.758
CuIr	1.744	-0.532	-1.197	0.000	-0.706
RuIr	1.732	-0.243	-1.103	0.019	-0.411
CrNi	1.533	-0.377	-0.729	-0.209	-0.513
NiNi	1.566	-0.037	-0.639	0.000	-0.258
NiCu	1.575	-0.196	-0.644	-0.225	-0.247
CrIr	1.637	-0.179	-1.057	-0.236	-0.274
CrCr	1.799	-0.004	-0.563	0.069	-0.004
CrCu	1.591	-0.328	-0.765	-0.055	-0.502
CuCu	1.562	-0.122	-0.722	0.008	-0.444

Table S4. Detailed analysis of water adsorption on MN-gCN surfaces. This table provides a comprehensive dataset for H_2O interaction with various transition metal (TM) on MN-gCN surfaces. It includes the metal pair (MN), the TM involved in the primary interaction with H_2O (H_2O-TM), the distance between H_2O and TM (H_2O-TM distance in Å), the Bader charge of H_2O*, and the integrated crystal orbital Hamilton population (iCOHP) for the H_2O-TM interaction.

MN	H_2O-TM	H_2O-TM distance (eV)	H_2O* Bader charge (e)	H_2O-TM iCOHP (eV)
FeFe	O-Fe	2.236	0.015	-0.399
MnFe	O-Fe	2.190	0.024	-0.378
FeCu	O-Fe	2.177	0.043	-0.367
FeNi	O-Fe	2.160	-0.022	-0.405
FePd	O-Fe	2.358	-0.022	-0.308
FePt	O-Fe	2.388	-0.095	-0.273
FeCo	O-Fe	2.190	0.037	-0.356
FeIr	O-Fe	2.304	-0.023	-0.248
CoNi	O-Co	2.118	0.029	-0.390
CoPt	O-Co	2.319	-0.071	-0.280
CoPd	O-Co	2.076	-0.003	-0.420
CoIr	O-Co	2.116	-0.117	-0.411
CoCu	O-Co	2.182	-0.013	-0.431
CrCo	O-Co	2.091	-0.003	-0.473
CoCo	O-Co	2.094	0.019	-0.385
CrFe	O-Cr	2.254	0.052	-0.962
CrNi	O-Cr	2.267	0.006	-0.398
CrPt	O-Cr	2.828	-0.115	-0.098
CrCr	O-Cr	2.058	0.002	-0.829
CrMn	O-Cr	2.093	0.026	-0.704
CrIr	O-Cr	2.098	-0.011	-0.766
CrRu	O-Cr	2.214	-0.036	-0.648
CrCu	O-Cr	2.383	0.004	-0.374
CrPd	O-Cr	2.523	-0.040	-0.177
MnMn	O-Mn	2.204	0.010	-0.464
MnIr	O-Mn	2.220	-0.009	-0.418
MnRu	O-Mn	2.390	-0.047	-0.415
MnNi	O-Mn	2.337	-0.080	-0.337
MnCu	O-Mn	2.264	0.022	-0.314
MnPt	O-Mn	2.392	-0.116	-0.281
MnPd	O-Mn	2.329	0.002	-0.268
MnCo	O-Mn	2.281	-0.011	-0.294
PtRu	O-Ru	2.118	-0.014	-0.791
CuRu	O-Ru	2.232	0.010	-0.753
NiRu	O-Ru	2.441	-0.024	-0.542
FeRu	O-Ru	2.253	0.012	-0.716
PdRu	O-Ru	2.263	-0.016	-0.726
CoRu	O-Ru	2.217	0.010	-0.661
RuRu	O-Ru	3.378	-0.249	-0.007

NiIr	O-Ir	3.231	-0.172	0.000
IrIr	O-Ir	2.864	-0.126	-0.119
PtIr	O-Ir	2.217	-0.489	-0.822
RuIr	O-Ir	2.554	-0.040	-0.330
CuIr	O-Ir	2.409	-0.007	-0.187
NiPd	O-Ni	2.593	-0.055	-0.107
NiPt	O-Ni	2.641	-0.108	-0.078
NiNi	O-Ni	2.332	-0.019	-0.129
PdIr	O-Pd	3.114	-0.184	0.003
PdPt	O-Pd	2.939	-0.163	-0.032
PdPd	O-Pd	2.898	-0.169	-0.082
CuPd	O-Cu	2.454	-0.001	-0.115
CuPt	O-Cu	2.546	-0.190	-0.128
CuCu	O-Cu	2.234	-0.047	-0.261
NiCu	O-Cu	2.413	-0.017	-0.542
PtPt	O-Pt	3.192	-0.240	-0.005

Table S5. Comparative Adsorption Energies for Different Metal Combinations. This table presents the adsorption energies (ΔG) in eV for water (H₂O*), hydroxyl (H*-OH*), and hydroxide (OH*) on various SAD surfaces. Each row corresponds to a unique metal combination (MN), showing how their interaction influences the adsorption energy of these three species.

MN	$\Delta G_{(H2O*)}$ (eV)	$\Delta G_{(H*-OH*)}$ (eV)	$\Delta G_{(OH*+1/2H2)}$ (eV)
FeFe	-0.891	0.616	-0.31
MnFe	-0.594	-0.132	-0.418
FeCu	-0.401	0.002	-0.007
FeNi	-0.381	0.267	-0.017
FePd	-0.309	0.662	-0.251
FePt	-0.285	0.509	0.198
FeCo	-0.243	0.044	-0.62
FeIr	0.001	-0.457	-0.079
CoNi	-0.736	0.68	-0.359
CoPt	-0.42	0.554	-0.239
CoPd	-0.292	0.828	-0.217
CoIr	-0.203	-0.46	0
CoCu	-0.167	0.48	-0.833
CrCo	-0.139	-0.516	-0.495
CoCo	-0.107	-0.325	-0.386
CrFe	-0.863	-0.434	0.048
CrNi	-0.768	0.319	-0.168
CrPt	-0.71	-0.05	-0.099
CrCr	-0.656	0.131	-0.036
CrMn	-0.633	0.5	-0.917
CrIr	-0.612	-0.197	0.636
CrRu	-0.49	-0.937	0.265
CrCu	-0.187	-0.332	-0.326
CrPd	-0.055	-0.304	0.075
MnMn	-0.5	-0.441	-0.704
MnIr	-0.445	-0.267	0.317
MnRu	-0.375	-0.467	-0.002
MnNi	-0.309	0.363	-0.372
MnCu	-0.261	-0.225	-0.037
MnPt	-0.255	0.49	-0.236
MnPd	-0.235	0.467	-0.082
MnCo	-0.211	-0.098	-0.368
CuRu	-0.634	-0.14	0.074
NiRu	-0.535	-0.344	0.388
FeRu	-0.433	-0.221	0.05
PtRu	-0.387	-0.06	-0.426
PdRu	-0.359	0.226	-0.444
CoRu	-0.115	-0.811	-0.2
RuRu	-0.057	-0.206	0.242
NiIr	-0.604	0.441	-0.188
IrIr	-0.339	-0.534	0.421

PtIr	-0.141	0.175	0.092
RuIr	0.133	-0.815	0.354
CuIr	-0.016	-0.187	0.158
NiPd	-0.006	0.639	0.464
NiPt	0.035	1.037	-0.293
NiNi	0.1	0.396	-0.296
PdIr	-0.14	0.403	-0.317
PdPt	0.091	0.518	0.463
PdPd	0.053	1.457	-0.224
CuPd	-0.188	0.376	0.622
CuPt	-0.118	0.789	-0.169
CuCu	-0.086	-0.08	-0.131
NiCu	-0.018	-0.131	-0.014
PtPt	-0.039	1.578	-0.141

Detailed Analysis of the Electronic Descriptor (φ) in Catalysis

Within the framework of our study, the electronic descriptor (φ) emerges as a pivotal indicator for evaluating and predicting the catalytic activity of transition metal-based catalysts, particularly in the context of the Hydrogen Evolution Reaction (HER). This descriptor is meticulously derived from two fundamental properties of transition metals: the number of d electrons (N_d) and their electronegativity (E_{TM}). The integration of these parameters into φ allows for a comprehensive assessment of the electronic environment and its impact on the catalytic functionality of dual-atom catalysts (DACs).

The number of d electrons (N_d) significantly influences the density of states at the Fermi level, which is crucial for the adsorption of reactants and the subsequent catalytic processes. Electronegativity (E_{TM}), on the other hand, affects the strength of the adsorptive bond between the catalyst surface and the reactants or intermediates, thereby influencing the activation barriers and the desorption of reaction products. The descriptor φ, therefore, encapsulates the interplay between these electronic properties, guiding the optimization of catalyst design for enhanced HER performance.

To provide a deeper understanding of the role of φ in catalysis, this section of the Supplementary Information includes a series of computational analyses that demonstrate the relationship between the φ values and the catalytic efficiency observed in various DACs. By highlighting the correlation between specific φ values (derived from N_d and E_{TM}) and the enhanced activity in HER, we aim to underscore the predictive power of this electronic descriptor in identifying high-performance catalysts.

This detailed exposition on the electronic descriptor (φ), derived from the integration of N_d and E_{TM}, enriches our understanding of the electronic factors that govern the catalytic activity of transition metals. By delving into the significance of φ in the catalytic process, especially in the realm of hydrogen production, we contribute to the foundational knowledge necessary for the rational design and development of next-generation catalysts for sustainable energy technologies.

Table S6. Descriptor and Reactivity Parameters for Metal Dimers on gCN. This table lists the calculated descriptor (
$$\varphi = \frac{N_d}{\sqrt{E_{TM}}}$$
), which combines the d electron count (N_d) and the electronegativity (e_{TM}) of transition metal (TM) atoms, dissociation energy (E_{diss}), and activation energy (E_a) for various homonuclear and heteronuclear metal dimers supported on g-CN. The descriptor φ serves as a simplified indicator of the electronic properties influencing the reactivity of the dimers.

MN	φ	E_{diss} (eV)	E_a (eV)
CoCo	5.11	-0.765	1.103
CuCu	7.25	-0.162	1.179
CrCu	5.62	-0.641	1.558
CrCo	4.51	-0.769	0.421
MnMn	4.02	-0.828	0.631
MnCo	4.58	-0.615	0.924
NiCu	6.52	-0.048	2.313
MnCu	5.71	-0.828	1.245
FeRu	4.58	-1.096	0.328

|			
FeCo	4.77	-0.28	1.925
NiNi	5.79	0.356	2.095
PtIr	5.35	0.254	0.749
PtRu	5.35	0.185	0.995
CuIr	5.94	-0.255	1.284
FeIr	4.58	-1.407	0.417
CrPd	5.4	-0.918	1.775
FeCu	5.86	-0.574	1.602
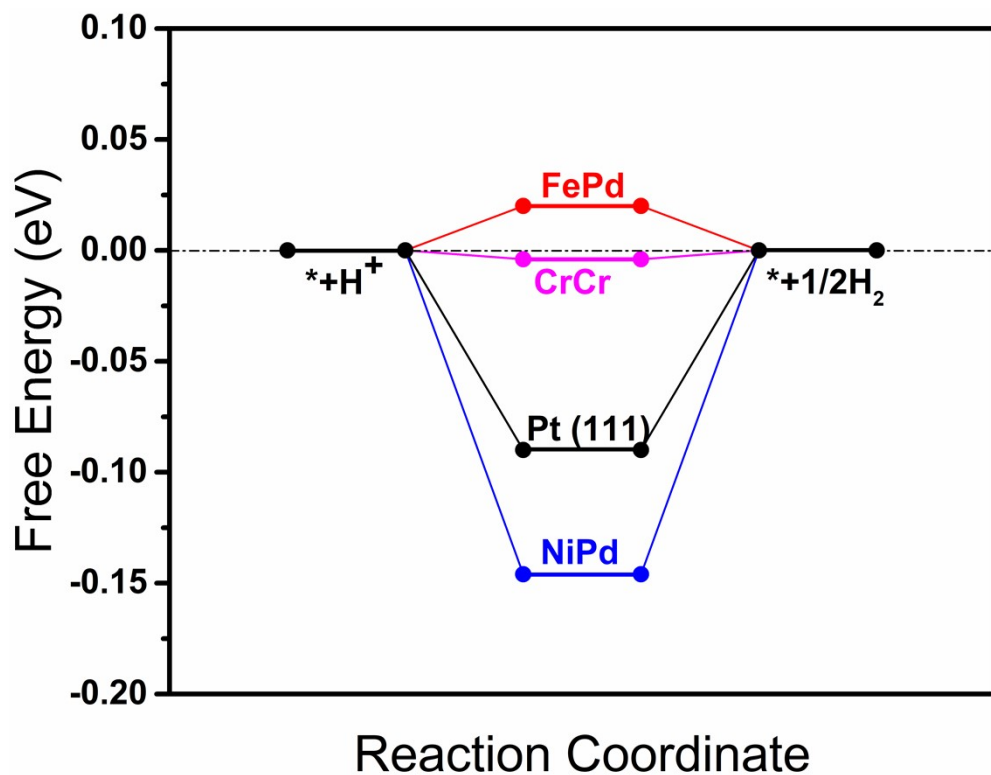
Figure S1. Free energy diagrams for hydrogen adsorption at active sites of FePd-gCN (0.02eV), CrCr-gCN (-0.004eV), NiPd-gCN (-0.146eV), and Pt(111) (-0.09eV)[S1].
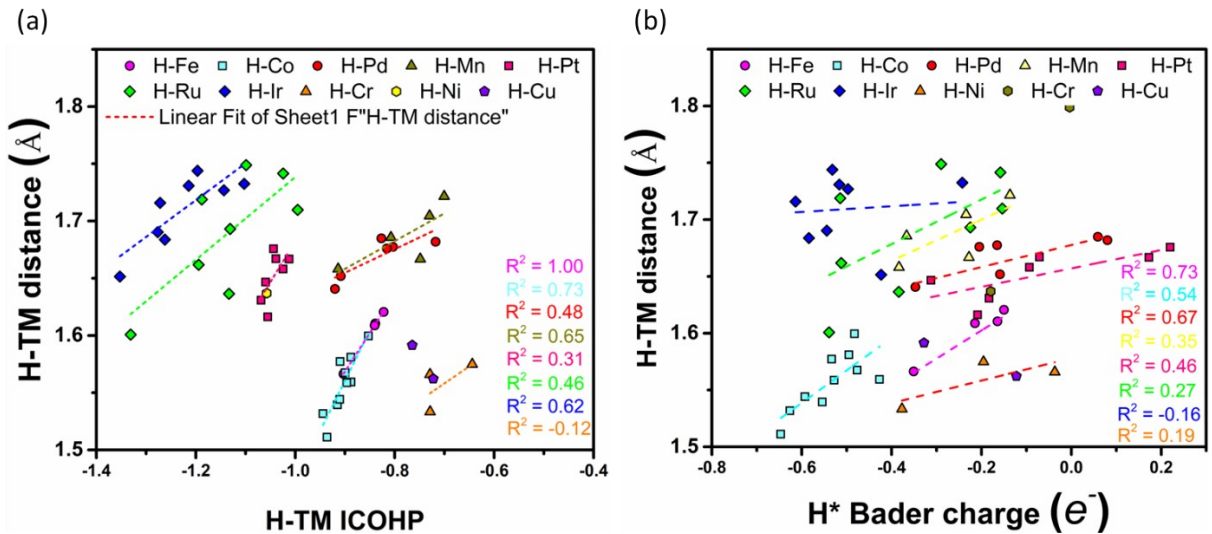
Figure S2. Comparative analysis of H-TM distance versus electronic properties for various transition metals (TM) bonded with hydrogen. (a) illustrates the relationship between H-TM bond distance and H-TM integrated crystal orbital Hamilton population (ICOHP), with each point representing a different TM-H pair. (b) demonstrates the correlation between H-TM distance and the Bader charge H*.
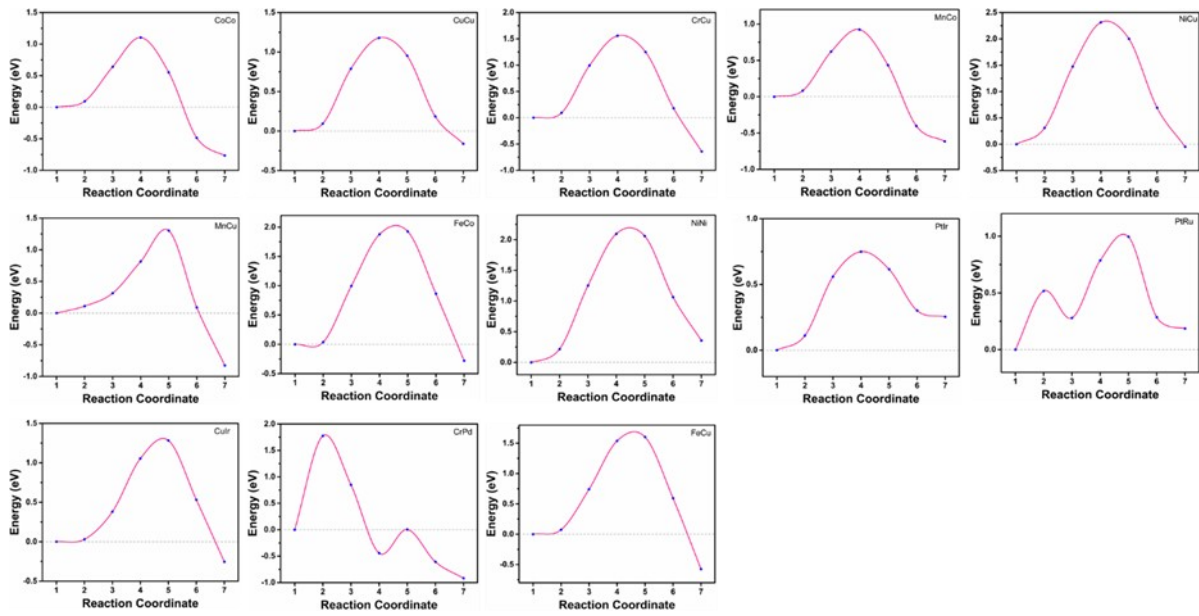
Figure S3. Computed energy barriers for H_2O dissociation on selected MN-gCN surfaces. This figure illustrates the results of the Nudged Elastic Band (NEB) method calculations, showing the energy barriers for water dissociation on various MN-gCN surfaces that have been identified as energetically favorable based on free energy profiles. Each panel corresponds to a different metal dimer configuration on the gCN substrate, detailing the energy variation along the reaction coordinate.
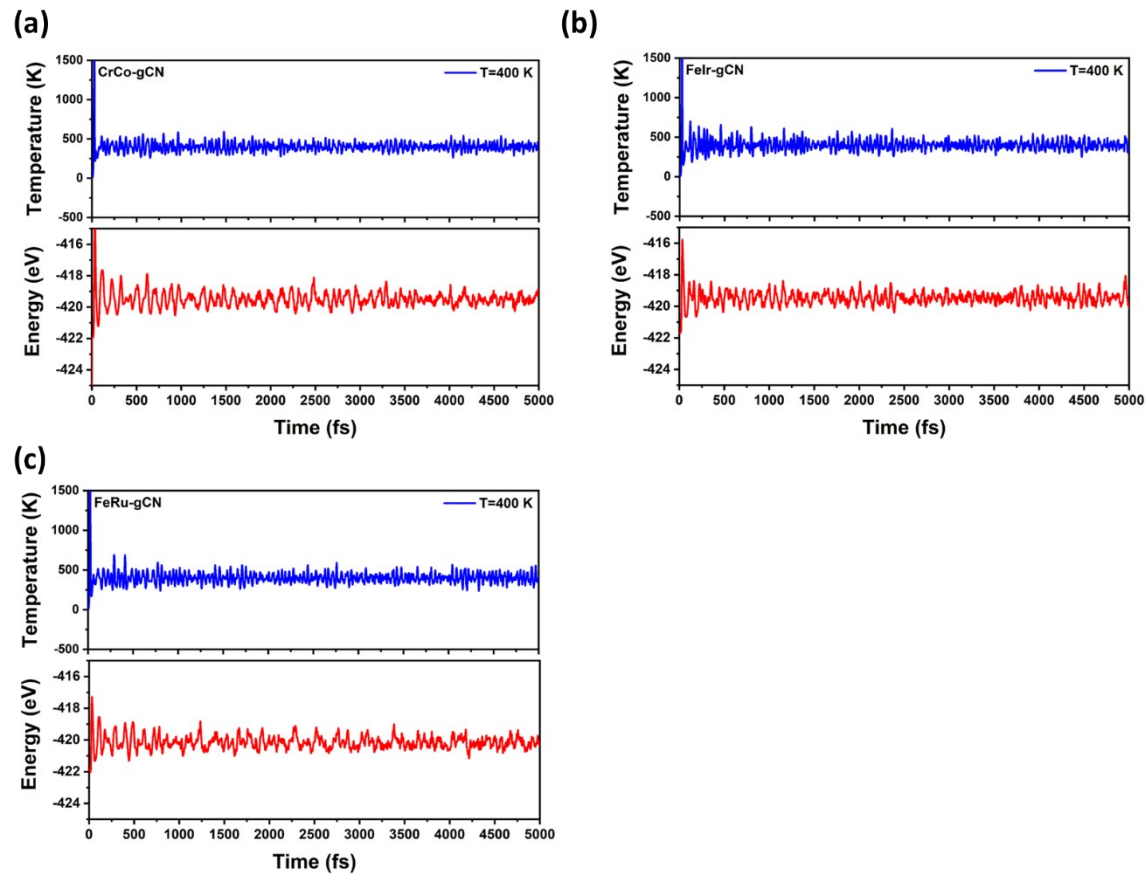
Figure S4. Molecular dynamics simulation results at 400 K for (a) CrCo-gCN, (b) FeIr-gCN, and (c) FeRu-gCN structures over 5000 fs. The upper panels show the temperature profiles and the lower panels display the total energy levels, validating the structural stability of the DACs on the defected g-CN substrate.

References

[S1]Wang, P., Zhang, X., Zhang, J. *et al.* Precise tuning in platinum-nickel/nickel sulfide interface nanowires for synergistic hydrogen evolution catalysis. *Nat Commun* **8**, 14580 (2017).